REVIEW

Electrocatalyst Characterization

ADVANCED
MATERIALS

www.advmat.de

Check for updates

X-Ray Absorption Spectroscopy Characterizations on PGM-Free Electrocatalysts: Justification, Advantages, and Limitations

Qingying Jia, Ershuai Liu, Li Jiao, Serge Pann, and Sanjeev Mukerjee*

Transition metals embedded in nitrogen-doped carbon matrices (denoted as M-N-C) are the leading platinum group metal (PGM)-free electrocatalysts for the oxygen reduction reaction (ORR) in acid, and are the most promising candidates for replacing platinum in practical devices such as fuel cells. Two of the long-standing puzzles in the field are the nature of active sites for the ORR and the reaction mechanism. Poor understanding of the structural and mechanistic basis for the exceptional ORR activity of M-N-C electrocatalysts impedes rational design for further improvements. Recently, synchrotron-based X-ray absorption spectroscopy (XAS) has been successfully implemented to shed some light on these two issues. In this context, a critical review is given to detail the contribution of XAS to the advancement of the M-N-C electrocatalysis to highlight its advantages and limitations.

1. Introduction

Thanks to the rapid development of synchrotron light sources around the world, synchrotron-based X-ray absorption spectroscopy (XAS) has emerged as an important and popular characterization technique in many fields including biology, materials science, and electrochemistry. If properly implemented, XAS can provide unique insights into the local structure in atomic scale and electronic properties in subtle details of measured materials, and is thus a powerful technique to elucidate the structure–performance correlations of materials with complex structures. A representative example is the recent XAS applications in advancing the field of platinum group metal (PGM)-free electrocatalysts for the oxygen reduction reaction (ORR), which will be briefly introduced here with the specific aims of 1) highlighting the unique advantages of XAS and its essential roles in elucidating the nature of active sites and the ORR

Prof. Q. Jia, E. Liu, Dr. S. Pann, Prof. S. Mukerjee
Department of Chemistry and Chemical Biology
Northeastern University
Boston, MA 02115, USA
E-mail: s.mukerjee@neu.edu
L. Jiao
Department of Chemical Engineering
Northeastern University
Boston, MA 02115, USA

The ORCID identification number(s) for the author(s) of this article can be found under https://doi.org/10.1002/adma.201805157.

mechanisms; 2) contributing to proper and rigorous application of XAS in this field by marking the fundamental and practical limitations of XAS.

2. In Situ XAS

A recent breakthrough in XAS characterizations on PGM-free electrocatalysts was the actualization of in situ XAS study by Mukerjee's and other groups.[1–7] In situ XAS allows for identification of electronic and structural properties of active sites during the ORR rather than ex situ under vacuum or exposed to air, thus provides more relevant and enriched insights into active sites structure and reaction mechanisms. They observed that the XAS signals, including both the extended X-ray absorption fine structure (FT-EXAFS) and X-ray absorption near edge structure (XANES) spectra, shift monotonically with applied potentials in both acid (**Figure 1**a,b)[3,4,6,8] and alkaline[5] for most of Fe-N-C electrocatalysts[1]; but not for Co-N-C electrocatalysts (Figure 1c,d).[8,9] Accordingly, the redox transition (H)O-Fe^{3+}-N_4 ↔ Fe^{2+}-N_4 during the ORR wherein the oxygen adsorbate (denoted as O(H)) generated from the ORR and/or the water activation was proposed to account for the shift of XAS signals with potentials. Specifically, the Fe^{3+}/Fe^{2+} transition reasonably explain the negative shift of the XANES edge with decreasing potentials (Figure 1a), and the associated desorption of the oxygen adsorbate accounts for the reduced intensity of the Fe-N/O scattering peak around 1.5 Å (Figure 1b). The direct observation of the redox transition of Fe^{2+}-N_4 active sites during the ORR constitutes the core finding of in situ XAS and leads to three important contributions in the M-N-C electrocatalysis for the ORR.

The first one is the establishment of the redox mechanism associated with the dynamic site-blocking effect.[3,6] It has long been recognized that the onset potentials of the ORR polarization of a broad variety of Fe-N-C electrocatalysts coincide with their Fe^{3+}/Fe^{2+} redox potentials,[4–6,10] and accordingly the redox mechanism was proposed to underscore the critical role of the redox potential on dictating the ORR activity.[11] However, this key observation had not been rationalized until lately by the potential dependent site-blocking effect associated with the Fe redox transition.[3] This notion was derived from the in situ XAS observations that the number of unoccupied Fe-N_4 active sites sharply changes when the potential scans across the Fe^{3+}/Fe^{2+} redox potential *as per* Equation (1)

$$N_{\text{active}} = N_{\text{total}} \frac{1}{1 + e^{\frac{F}{RT}(E - E_{\text{redox}})}} \qquad (1)$$

where N_{active} and N_{total} are the available and total number of surface active sites, respectively; F, R, and T take the usual meanings; E is the cathode potential, E_{redox} is the redox potential under the relevant operation conditions. The curves of the $N_{\text{active}}/N_{\text{total}}$ as a function of potentials derived from Equation (1) based on the experimental E_{redox} of both pyrolyzed and unpyrolyzed Fe-N-C electrocatalysts match well with the ORR polarization curves (Figure 1e). This finding indicates that the ORR activity of the Fe-N-C electrocatalysts is dictated by the Fe^{3+}/Fe^{2+} redox potential via the site-blocking effect. For example, more than 99% of the $Fe-N_4$ sites with a redox potential of 0.78 V_{RHE} is poisoned by the oxygen species at 0.9 V according to Equation (1), and only 50% will be poisoned if the redox potential is upshifted to 0.9 V. Later on, the redox mechanism in association with the site-blocking effect was expanded to Co-N-C and PGM electrocatalysts with a broad range of redox potential by establishing a general asymmetric volcano trend in the ORR activity: the ORR of the catalysts on the high redox potential side (or equivalently weak M—O binding energy) of the volcano is limited by the intrinsic activity; whereas the ORR of the catalysts on the low redox potential side (or equivalently strong M—O binding energy) is limited by either the site-blocking effect and/or intrinsic activity depending on the redox potential (Figure 1f).[9] Note that the real time monitor of the structural and electronic properties of the electrode and the coverage of the ORR intermediates as a function of applied potentials by in situ XAS makes it more than a characterization technique but also an analytical technique for mechanistic study.

The second contribution is the elucidation of the redox-induced structural-switching behavior of $Fe-N_4$ sites in pyrolyzed Fe-N-C samples.[3,6] By combining the XANES and the Fourier Transform (FT) of the EXAFS analysis, Jia et al.[3] found that the intact macrocycles such as the iron phthalocyanine (FePc) possess a typical square-planar $Fe^{2+}-N_4$ structure (D_{4h} symmetry), and the Fe^{2+} appears to move out of the plane upon the adsorption of oxygen species (**Figure 2**a). On the contrary, the Fe^{2+} ion is located off the N_4-plane moiety in pyrolyzed samples, and moves back into the plane when transiting to Fe^{3+} upon the adsorption of oxygen species (Figure 2b). Density functional theory (DFT) calculations suggest that the off-plane configuration suppresses the Fe-to-ligand back-donation of electrons, resulting in the enrichment of the d-electrons in the Fe center, and thus higher redox potential.[3] This prediction agrees with the experimental observation by Kramm et al.[12] that high pyrolysis temperature causes a partial donation of electron density from the N neighbors to the Fe in the $Fe-N_4$ moiety. DFT calculations further suggest that the switching from the off-plane to in-plane configuration of the pyrolyzed $Fe-N_4$ moieties is beneficial for the ORR kinetics by the weakening the overly strong Fe—O binding energy throughout the ORR process (Figure 2c). These results together provide a plausible explanation why the $Fe-N_4$ moiety formed upon high temperature pyrolysis has a higher redox potential and better inherent ORR activity than the unpyrolyzed $Fe-N_4$ macrocycles.

The third contribution of in situ XAS is that it arouses the reinterpretation of previous ex situ characterization results

Qingying Jia (MS and BS in physics from Beijing University) is currently a research assistant professor at Northeastern University. Dr. Jia obtained his Ph.D. in material sciences at Illinois Institute of Technology, USA, in 2010. Dr. Jia's research centers on synchrotron-based in situ X-ray absorption spectroscopy studies in electrochemistry.
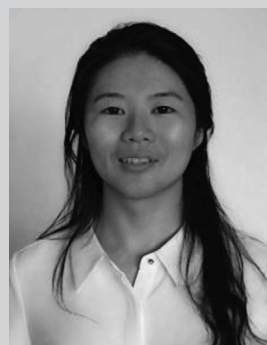
Li Jiao is a graduate student in the Department of Chemical Engineering at Northeastern University with a B.S. in material sciences. She is currently a graduate researcher at NUCRET working on PGM-free electrocatalysis.

Sanjeev Mukerjee is a professor in the Department of Chemistry and Chemical Biology (Northeastern University), where he has been since September 1998. He also heads the newly created center for Renewable Energy Technology and its subset, the Laboratory for Electrochemical Advanced Power (LEAP).

on the nature of active sites in Fe-N-C electrocatalysts. The in situ XAS signals of Fe-N-C electrocatalysts change dramatically with potential, reflecting the changes of the local structure and valence state of the $Fe-N_4$ moieties (Figure 1). It naturally brings about a key question: what is the form of the $Fe-N_4$ moieties seen ex situ? The answer to this question is crucial since nowadays most characterizations are still conducted ex situ exposed to air, and it is essential to verify whether the structure identified ex situ is relevant to the ORR activity measured in situ. It was clearly observed that the ex situ XAS signals nearly overlap the in situ ones collected at elevated potentials such as 0.9 V (Figure 1a,b),[6] which indicates that the $Fe^{2+}-N_4$ moieties at ex situ conditions exposed to air are in the form of $(H)O-Fe^{3+}-N_4$ (Figure 2d). This finding shows that the sites detected ex situ are actually the active sites occupied by oxygen adsorbates ($(H)O-Fe^{3+}-N_4$), rather than the clean active sites

ADVANCED
SCIENCE NEWS
www.advancedsciencenews.com

ADVANCED
MATERIALS
www.advmat.de
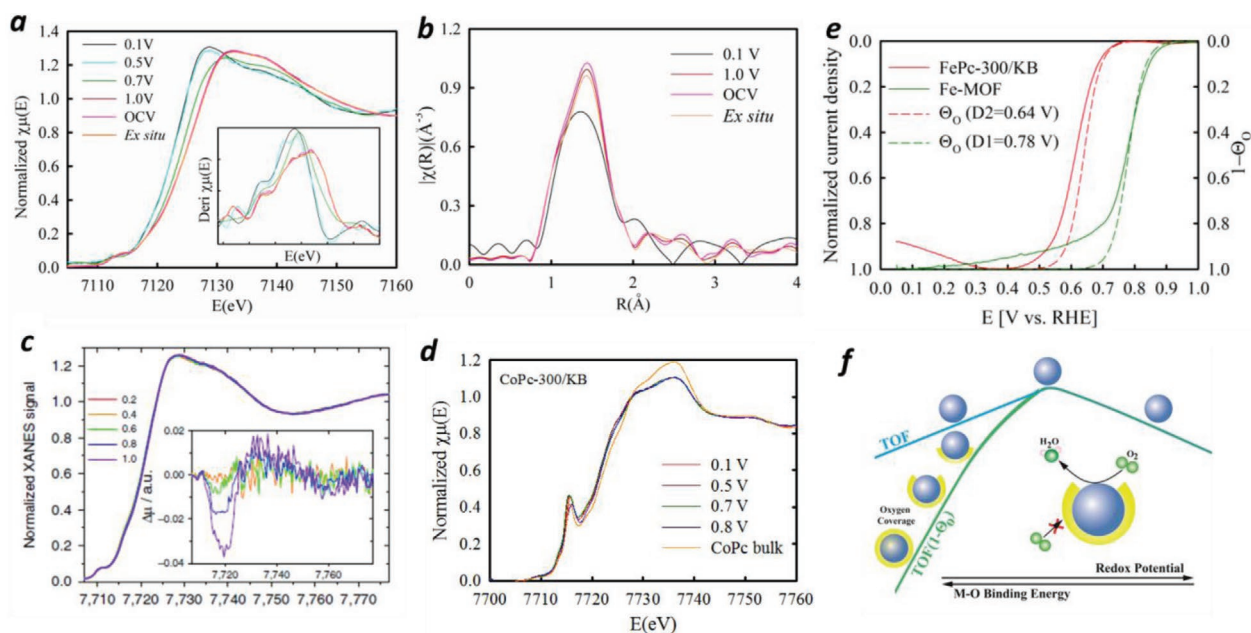
Figure 1. Ex situ and in situ a) XANES and b) FT-EXAFS of the FePhenMOF-ArNH₃ electrocatalyst. Ex situ data were first collected on the dry electrode, and the in situ spectra were collected at 0.1–1.0 V on the same electrode in O_2-saturated 0.1 M $HClO_4$ at room temperature; c) operando XANES spectra of $Co_{0.5}$ taken in a 0.5 M O_2-saturated H_2SO_4 electrolyte as a function of the electrochemical potential; d) in situ XANES of CoPc-300/KB collected at 0.1–0.8 V in a O_2-saturated 0.1 M $HClO_4$ electrolyte; e) Normalized ORR kinetic current of FePc-300/KB and Fe-MOF in comparison with the oxide coverage derived from Equation (1) using the experimental redox potential of 0.78 and 0.64 V, respectively; f) scheme of the asymmetric volcano curve of the turnover frequency (TOF) of electrocatalysts with a wide range of the redox potential or equivalently the binding energy to oxygen. a,b) Reproduced with permission.[6] Copyright 2016, Royal Society of Chemistry. c) Reproduced with permission.[8] Copyright 2017, Nature Publishing Group. d–f) Reproduced with permission.[9] Copyright 2017, American Chemical Society.
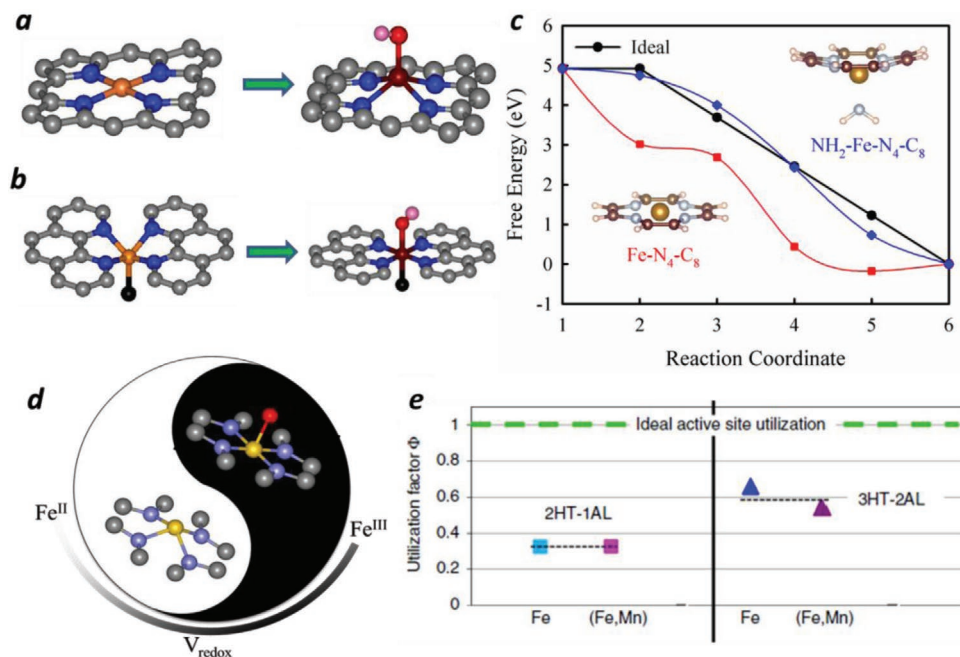
Figure 2. The Fe—N switching behavior of the a) in-plane and b) out-of-plane Fe-N₄ moieties with/without axially bound O(H)$_{ads}$; c) reaction coordinates correspond to the given systems: (1) *+O_2 + 4H⁺ + 4e⁻, (2) *OO + 4H⁺ + 4e⁻, (3) *OOH + 3H⁺ + 3e⁻, (4) *O + 2H⁺ + 2e⁻ + H_2O, (5) *OH + H⁺ + e⁻ + H_2O, (6)* + 2H_2O at a potential of 0 V relative to the hydrogen electrode. d) The Fe—N switching behavior of the out-of-plane Fe-N₄ moiety governed by the $Fe^{2+/3+}$ redox potential. The Fe, N, C, and O atoms are represented by yellow, blue, gray, and red spheres, respectively. e) The active-site utilization factor is plotted for the Fe-N-C and (Fe,Mn)-N-C electrocatalysts with 3HT-2AL. a–c) Reproduced with permission.[3] Copyright 2015, American Chemical Society. d) Reproduced with permission.[6] Copyright 2016, Royal Society of Chemistry. e) Reproduced with permission.[13] Copyright 2015, Nature Publishing Group.

ADVANCED
SCIENCE NEWS
www.advancedsciencenews.com

ADVANCED
MATERIALS
www.advmat.de

(Fe^{2+}-N_4) responsible for the ORR activity. Consequently, (H)O-Fe^{3+}-N_4 has been erroneously assigned as the active site for the ORR based on ex situ characterization results. Moreover, not all the Fe-N_4 sites embedded in 3D carbon matrix are accessible by air (Figure 2e).[13] The moieties buried underneath the surface are in the form of Fe^{2+}-N_4 whereas the moieties exposed to air are in the form of (H)O-Fe^{3+}-N_4 owing to the strong Fe—O binding energy. The two species are copresent in Fe-N-C samples, and detected by bulk average techniques such as XAS or Mossbauer. This poses another question whether the multiple moieties seen by Mossbauer are really different type of active centers as widely assumed thus far, or just the same center with/without oxygen adsorbate? Li et al.[6] recently seconded the latter case given that Mössbauer cannot distinguish between zero-spin Fe^{2+}-N_4 and high-spin Fe^{3+}-N_4 moieties.[14] Apparently, the interpretation of ex situ characterization results should be implemented with caution to account for in situ results. It is noted that this is the issue only for Fe-N_4 or sites located in the strong M—O binding leg of the volcano curve such as Mn-N_4,[15] but not for sites located in the weak M—O binding leg like Co-N_4 or Ni-N_4 (Figure 1f) since they do not get oxidized even exposed to air.[9,16]

Overall, the in situ XAS characterizations suggest that the redox mechanism associated with the site-blocking effect is the governing mechanism for the M-N-C ORR electrocatalysts dominated with M-N_4 moieties, and the redox potential is a good descriptor of the ORR activity in acid. The redox potential is tunable by tuning the local geometry of M-N_4 moieties, but

Table 1. Summary of the characteristic features of the XANES spectra of the M-N_4-C moieties and their energy, assignment, and diagnose.

Feature	Energy [eV]	Assignment	Diagnose
A	7112	$1s \rightarrow 3d$ allowed by p-d hybridization	D_{4h} symmetry
B	7117	$1s \rightarrow 4p_z$	D_{4h} symmetry
C	7128	$1s \rightarrow 4p_{xy}$	R_{Fe-N}
D	7139	multiple scattering $Fe \rightarrow N \rightarrow Fe \rightarrow N'$	R_{Fe-N}
E	7153–7162	first coordination shell scattering	R_{Fe-N}

the precise control over the local structure has not been realized yet. The ORR mechanism of the M-N-C electrocatalysts in alkaline is different from that in acid,[17] and is beyond the scope of this article.

3. XANES Analysis

Like many other spectroscopic techniques, the XANES is essentially a fingerprint technique that probes the oxidation state and coordination environment of the absorbing atom. In particular, the energy position, splitting, and intensity distribution of the XANES features of Fe-centered compounds change
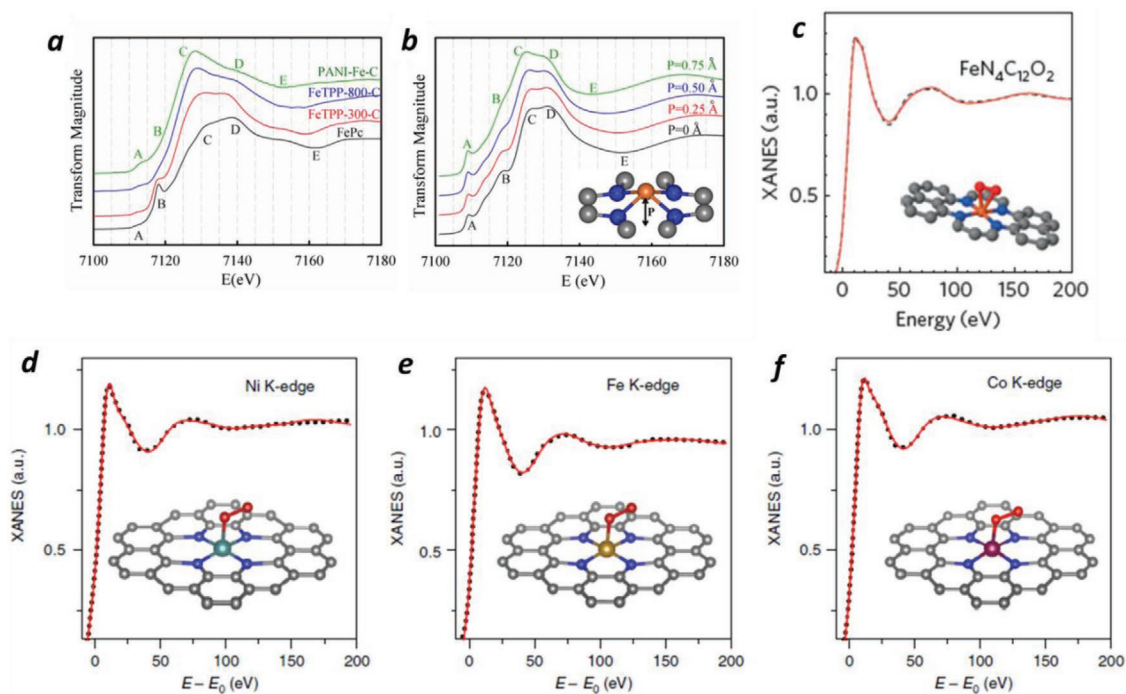
Figure 3. a) The XANES spectra of Fe-N-C electrocatalysts collected at 0.1 V in N_2-saturated 0.1 M $HClO_4$; b) the XANES spectra calculated by FEFF9 based on the Fe-N_4-C_8 model with various central Fe displacements (denoted as P). c) Comparison between the K-edge XANES experimental spectrum of $Fe_{0.5}$ (black dashed lines) and the theoretical spectrum calculated with the FeN_4C_{12} moiety with one O_2 molecule adsorbed in side-on mode (solid red lines). d–f) Comparison between the experimental XANES spectra (black dotted lines) for M-NHGFs and the best-fit theoretical spectra (solid red lines). The insets show the geometrically refined MN_4C_4 structure. a,b) Reproduced with permission.[3] Copyright 2015, American Chemical Society. c) Reproduced with permission.[23] Copyright 2015, Nature Publishing Group. d–f) Reproduced with permission.[24] Copyright 2018, Nature Publishing Group.

**ADVANCED
SCIENCE NEWS**

www.advancedsciencenews.com

**ADVANCED
MATERIALS**

www.advmat.de

systematically with the spin state, oxidation state, and local geometry.[18] Diagnosis of the XANES features, when combined with advanced theoretical calculations and reliable reference spectra, can provide valuable information of the local geometry and electronic configuration of the absorbing atom. Jia et al.[3] found that the XANES of the Fe-N-C electrocatalysts can be defined by five characteristic features that are ultrasensitive to the local symmetry of the Fe-N$_4$ moiety and the Fe—N bond distance ($R_{\text{Fe−N}}$) (**Table 1**), and these features can be well captured by the FEFF9 program. This program allows for *ab initio* multiple-scattering calculations of XAS spectra of clusters,[19] on the basis of the Fe-N$_4$-C$_x$ models (**Figure 3**a,b). They noticed that as the iron meso-tetraphenylporphyrine chloride (FeTPPCl) are pyrolyzed with increasing temperature, their characteristic XANES features exhibit monotonic trends in amplitude and/or position, approaching to those of the state-of-the-art Fe-N-C electrocatalyst[20] synthesized from separated Fe, N, and C precursors (Figure 3a). These trends can be reproduced in the FEFF9-generated XANES by moving the central Fe away from the N$_4$-plane, and fully accounted for by the distortion of the D_{4h} symmetry and/or the increase in $R_{\text{Fe−N}}$ as consequences of the Fe out-of-plane displacement (Figure 3b).[3] This comparison study provides strong evidence that a key difference between unpyrolyzed Fe-N$_4$ moieties and pyrolyzed ones is that the former possesses an in-plane configuration whereas the latter has a distorted out-of-plane configuration.

The FEFF-based XANES study has been limited to qualitative analysis by far, partly because of the fundamental difficulty in actually fitting the spectrum of 2D structures like the in-plane Fe-N$_4$. Recent development in the Ensemble-Learned Spectra IdEntification (ELSIE) algorithm makes FEFF achieve up to 84.2% accuracy in identifying the oxidation state and coordination environment of the K-edge XANES spectra up to 19 elements,[21] which allows for future quantitative XANES analysis of M-N-C electrocatalysts.

Semi-quantitative XANES analysis is practically feasible by combining it with principle component analysis (PCA) or linear combination fitting (LCF) analysis as illustrated by Ferrandon et al.[22] However, the LCF requires some knowledge of the nature of active sites to guide the choice of reference materials, which is rarely the case for pyrolyzed M-N-C materials; whereas PCA does not require so, and is powerful to determine the number of components with relative fractions in pyrolyzed M-N-C materials.[22]

Recently, quantitative XANES fitting was realized by Frederic's[8,23] and Huang's[24] group on M-N-C (M = Fe, Co, and Ni) electrocatalysts (Figure 3c), and the cluster models derived from the XANES fitting were further confirmed by the EXAFS fitting. This technical advancement allows for quantitative identification of the local structure of M-N$_x$ moieties. Both groups found that the XANES of the Fe-N-C samples ex situ can be well fitted with an in-plane Fe-N$_4$ moiety with an axial O$_2$ molecule, in consistent with the results derived from in situ XAS study aforementioned. Huang's group further showed that the same configuration can be used to fit the Co-N-C and Ni-N-C electrocatalysts as well; whereas Frederic et al. showed that the calculated XANES of the Co-N$_4$ cluster model with or without axial O$_2$ matches the experimental XANES, and favored the case without axial O$_2$ based on the weak Co—O$_2$ binding as well

as the unchanged XANES within the potential range from 0 to 1.0 V (Figure 1c).[8] These results indicate that although the XANES spectrum is generally sensitive to the local coordination environment of the absorbing atom, it seems to be insensitive to the axial ligand of M-N$_4$ moieties and thus cannot be used to justify the existence of the axial ligand in M-N$_4$ moieties. Therefore, even though that M-N$_4$ and (H)O-M-N$_4$ moieties normally co-exist in M-N-C, the bulk average XANES can still be fitted with one M-N$_4$ cluster model with or without O$_2$. Complementary techniques such as in situ scanning tunneling microscope[25] are thus required to unambiguously identify the nature of active sites in M-N-C electrocatalysts.

4. FT-EXAFS Analysis

EXAFS fitting is a powerful technique that allows for the quantitative identification of the coordination number (*CN*), bond distance (*R*), and local orderness. It is thus extremely suitable for M-N-C electrocatalyst characterizations since these quantities largely define the local structure of M-N$_4$ moieties, and have been commonly used to justify their ORR performance. Despite these advantages of the EXAFS fitting, this technique

Table 2. Summary of the EXAFS fitting results of the bond distance and coordination number of the first shell Fe—N/O scattering in Fe-N-C electrocatalysts.

Separated Fe—N and Fe—O		Fe—N		Fe—O	
		CN	BD [Å]	CN	BD [Å]
FePc[26]		3.2	1.93		
FePc/BP[27]		3.0	1.93		
FePc-900/BP[27]		3.76	1.963		
Fe$^{0.5}$-900[23]		4	1.99	1	1.91
Fe$^{0.5}$-950[23]		4	2.01	1	1.92
Fe-NHGF[19]		4.1	1.98	0.9	2.16
FeTPPCl[5]		4.01	2.054	–	–
FeTPPCl/C HT300°C[5]	0.1 V	4.03	1.996	0.10	2.055
	0.9 V	4.00	2.059	1.00	1.873
FeTPPCl/C HT800°C[5]	0.1 V	4.00	1.976	0.61	1.797
	0.9 V	4.00	1.990	2.20	1.848

Mixed Fe—N/O		Fe—N/O	
		CN	BD [Å]
FeTPP	0.1 V	3.8	1.98
−300−C[3]	0.9 V	5.4	2.07
FeTPP	0.1 V	4.1	2.03
−800−C[3]	0.9 V	5.2	2.01
FePhenMOF-ArNH$_3$[6]	0.1 V	3.8	2.07
	1.0 V	5.4	1.98

| Inorganic Fe species		Fe—Fe	
Fe-MOF[2]	0.1–0.9V	6.8	2.51
		Fe—N/O	
		1.2	1.97

has some inherent limitations. Full awareness of these limitations is crucial for acquiring reasonable fitting and proper interpretation of the fitting results. Both the advantages and limitations of EXAFS analysis on M-N-C electrocatalysts will be elaborated below.

The EXAFS fitting results of the *CN* and *R* of the Fe−N/O bond in a variety of Fe-N-C electrocatalysts are summarized in **Table 2**. It is noted that only the samples with dominant Fe-N₄ moieties or inorganic metal species are present here. These two types of species can be distinguished by EXAFS fitting as the bond length of the Fe−Fe and Fe−N/O scatterings and the atomic number between Fe and N/O are sufficiently apart. Despite so, the EXAFS fitting of the samples with both species is less reliable although not technically infeasible. The key difference between these two species is that the XAS signals of Fe-N₄ moieties changes with potentials whereas those of inorganic Fe species do not, which indicates that the Fe-N₄ moieties are electrochemically active whereas the latter ones are not being encapsulated in carbon shells, and the N-doped carbon encapsulating inorganic Fe species was proposed as the active sites accordingly.[2]

As noticed, the EXAFS fitting was conducted either separating Fe−N and Fe−O bonds (top part in Table 2) or not (middle part in Table 2). The latter method is based on the inherent EXAFS limitations that N and O are indistinguishable by XAS as scattering neighbors, and the bonds with the bond distance variation within 0.2 Å are also indistinguishable. However, the former method can be justified by the XANES fitting conducted on the same sample aforementioned. The XANES fitting is also critical to reduce the number of fitting variables in the EXAFS fitting. A common issue for M-N-C samples is the relatively narrow range in both *k* (≈3–13 Å⁻¹) and *R* (1.0–2.2 Å) spaces owing to the lack of long range order scattering and the

light element neighbors (N and C). The narrow ranges in the K and R spaces lead to a limited number of independent points of ≈8, which allows for up to five variables to be fitted. Thus fixing some variables justified by other techniques is essential if fitting with multiple paths. Since the quantitative XANES fitting is still too advanced for general users, the determination of the cluster model for EXAFS fitting of the M-N-C electrocatalysts can be alternatively obtained by measuring the bulk MPc as a baseline model catalyst. This method also provides a reliable estimation of the amplitude reduction factor, which is essential for accurate determination of the *CN*. This principle also applies for the XANES analysis.

Despite the limitations of the EXAFS analysis, the EXAFS results obtained from different groups worldwide appear to converge to the conclusions that the Fe ion is surrounded by four nitrogen atoms, and the Fe−N bond distance at ex situ conditions is around 2 Å,[28] longer than that of FePc (1.93 Å) and FeTPP (1.97 Å). Since the Fe ion is located in the N₄-plane ex situ as suggested by EXAFS and XANES analysis, the longer Fe−N bond distance indicates the bigger cavity of the N-doped carbon matrix in the pyrolyzed Fe-N-C electrocatalysts compared to that in intact Fe-N₄ macrocycles. The *CN* of Fe−O bond at ex situ or elevated potentials is around 1. This fitting result, however, does not necessarily mean that each Fe-N₄ moiety attaches one axial O atom. It could be resulted from the bulk average of the Fe-N₄ moieties without axial O and the Fe-N₄ moieties with an O₂ adsorbate (corresponding to a Fe−O *CN* of 2),[23] or Fe-N₄ moieties with an atomic O adsorbate (corresponding to a Fe−O *CN* of 1) considering that the typical EXAFS fitting uncertainty of *CN* is around 1. In particular, Frederic's group[8,23] showed that both the cluster models with or without the axial O ligand can nicely fit the FT-EXAFS spectra of Fe-N-C and Co-N-C electrocatalysts (**Figure 4**), analogue of the XANES analysis. This
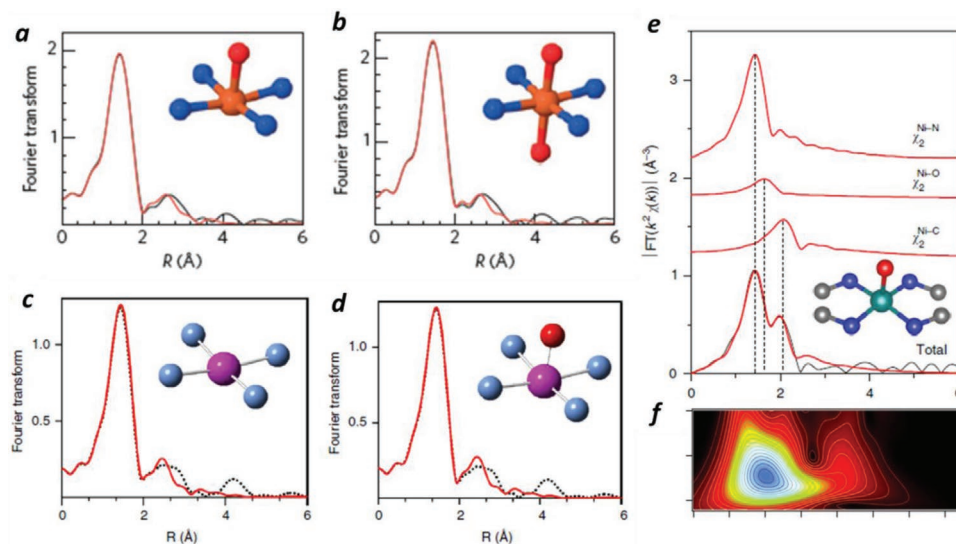
Figure 4. The fits of the Fe K-edge FT-EXAFS of Fe₀.₅ with a FeN₄ moiety having a) one or b) two oxygen atoms in the axial direction. The fits of the Co K-edge FT-EXAFS of Co₀.₅ with a FeN₄ moiety having c) zero or d) one oxygen atom in the axial direction. e) Ni K-edge EXAFS analysis of Ni-NHGF in the *R* space. Curves from top to bottom are the Ni−N, Ni−O, and Ni−C two-body backscattering signals χ₂ included in the fit and the total signal (red line) superimposed on the experimental signal (black line). f) Wavelet transforms for the k3-weighted EXAFS signals of M-NHGFs with optimum resolutions at 2.0 Å. The maxima at ≈4.0 Å⁻¹ are associated with the M-N/O/C contributions. a,b) Reproduced with permission.[23] Copyright 2015, Nature Publishing Group. c,d) Reproduced with permission.[7] Copyright 2017, Nature Publishing Group. e,f) Reproduced with permission.[24] Copyright 2018, Nature Publishing Group.

leaves some ambiguity in identifying the *CN* of M-N-C by XAS. In addition, the EXAFS fitting of M-N-C to the second shell of carbon atoms was realized by combining with the wavelet transforms of the EXAFS spectra (Figure 4).[24] It is worth noting that the Fe—O is absent at low potentials for Fe-N-C or negligible for bulk FePc ex situ with minimal fraction of FeN_4 exposed to air. These EXAFS fitting results together provide strong evidence that the surface Fe-N_4 moieties are covered by oxygen species ex situ, which directly support the site-blocking effect mentioned above.

5. Summary and Perspective

XAS has demonstrated its unique advantages in characterizing nanoscale materials with complex structures such as M-N-C electrocatalysts. It also allows for in situ characterization of electrodes under reactive conditions. The unique merits of XAS will be continuously boosted by the ongoing rapid advancement of the synchrotron sources worldwide and theoretical modeling programs. XAS can also contribute to understanding the instability of Fe-N-C electrocatalysts by monitoring the local structure and electronic property changes during the long-term fuel cell operation. From the XAS perspective, further improvements of M-N-C electrocatalysts for the ORR may be realized by increasing the inherent activity of M-N_4 sites via optimizing the redox potential or equivalently the M—O binding energy. By far the most active Fe-N_4 site has a redox potential around 0.78 V_{RHE} in 0.1 M $HClO_4$, ≈70 mV lower than that of Pt(111). Upshifting the redox potential of Fe-N_4 moiety may not only boost the inherent activity, but also dramatically alleviate the site-blocking effect. One possible way to upshift the Fe-N_4 redox potential is to increase the Fe—N bond distance. The second strategy is to enrich the abundance of M-N_4 sites accessible by O_2, which can be achieved by enriching the abundance of micropores in the carbon matrix and optimizing the morphology to maximum the exposure of M-N_4 sites. It is expected that XAS will grow into the next generation characterization technique in electrocatalysis and Materials Science.

Conflict of Interest

The authors declare no conflict of interest.

[1] Q. Jia, N. Ramaswamy, U. Tylus, K. Strickland, J. Li, A. Serov, K. Artyushkova, P. Atanassov, J. Anibal, C. Gumeci, S. C. Barton, M.-T. Sougrati, F. Jaouen, B. Halevi, S. Mukerjee, *Nano Energy* **2016**, *29*, 65.

[2] K. Strickland, E. Miner, Q. Jia, U. Tylus, N. Ramaswamy, W. Liang, M.-T. Sougrati, F. Jaouen, S. Mukerjee, *Nat. Commun.* **2015**, *6*, 7343.

[3] Q. Jia, N. Ramaswamy, H. Hafiz, U. Tylus, K. Strickland, G. Wu, B. Barbiellini, A. Bansil, E. F. Holby, P. Zelenay, S. Mukerjee, *ACS Nano* **2015**, *9*, 12496.

[4] U. Tylus, Q. Jia, K. Strickland, N. Ramaswamy, A. Serov, P. Atanassov, S. Mukerjee, *J. Phys. Chem. C* **2014**, *118*, 8999.

[5] N. Ramaswamy, U. Tylus, Q. Jia, S. Mukerjee, *J. Am. Chem. Soc.* **2013**, *135*, 15443.

[6] J. Li, S. Ghoshal, W. Liang, M.-T. Sougrati, F. Jaouen, B. Halevi, S. McKinney, G. McCool, C. Ma, X. Yuan, Z.-F. Ma, S. Mukerjee, Q. Jia, *Energy Environ. Sci.* **2016**, *9*, 2418.

[7] a) I. C. Stefan, Y. Mo, S. Y. Ha, S. Kim, D. A. Scherson, *Inorg. Chem.* **2003**, *42*, 4316; b) I. T. Bae, D. A. Tryk, D. A. Scherson, *J. Phys. Chem. B* **1998**, *102*, 4114.

[8] A. Zitolo, N. Ranjbar-Sahraie, T. Mineva, J. Li, Q. Jia, S. Stamatin, G. F. Harrington, S. M. Lyth, P. Krtil, S. Mukerjee, E. Fonda, F. Jaouen, *Nat. Commun.* **2017**, *8*, 957.

[9] J. Li, A. Alsudairi, Z.-F. Ma, S. Mukerjee, Q. Jia, *J. Am. Chem. Soc.* **2017**, *139*, 1384.

[10] J. H. Zagal, I. Ponce, D. Baez, R. Venegas, J. Pavez, M. Paez, M. Gulppi, *Electrochem. Solid-State Lett.* **2012**, *15*, B90.

[11] J. H. Zagal, M. Koper, *Angew. Chem., Int. Ed.* **2016**, *55*, 14510.

[12] U. I. Kramm, I. Abs-Wurmbach, I. Herrmann-Geppert, J. Radnik, S. Fiechter, P. Bogdanoff, *J. Electrochem. Soc.* **2011**, *158*, B69.

[13] N. R. Sahraie, U. I. Kramm, J. Steinberg, Y. Zhang, A. Thomas, T. Reier, J.-P. Paraknowitsch, P. Strasser, *Nat. Commun.* **2015**, *6*, 8618.

[14] F. Jaouen, Heat-Treated Transition Metal-N_xC_y Electrocatalysts for the O_2 Reduction Reaction in Acid PEM Fuel Cells, in *Non-Noble Metal Fuel Cell Catalysts* (Eds: Z. Chen, J. Dodelet, J. Zhang Dodelet), **2014**.

[15] a) Z. Lu, G. Xu, C. He, T. Wang, L. Yang, Z. Yang, D. Ma, *Carbon* **2015**, *84*, 500; b) W. Orellana, *J. Phys. Chem. C* **2013**, *117*, 9812.

[16] a) L. Osmieri, A. H. A. Monteverde Videla, P. Ocón, S. Specchia, *J. Phys. Chem. C* **2017**, *121*, 17796; b) X. X. Wang, D. A. Cullen, Y.-T. Pan, S. Hwang, M. Wang, Z. Feng, J. Wang, M. H. Engelhard, H. Zhang, Y. He, Y. Shao, D. Su, K. L. More, J. S. Spendelow, G. Wu, *Adv. Mater.* **2018**, *30*, 1706758; c) Q. Cheng, S. Han, K. Mao, C. Chen, L. Yang, Z. Zou, M. Gu, Z. Hu, H. Yang, *Nano Energy* **2018**, *52*, 485.

[17] a) S. Kim, H. Kim, *Catal. Today* **2017**, *295*, 119; b) N. Ramaswamy, S. Mukerjee, *J. Phys. Chem. C* **2011**, *115*, 18015; c) D. Malko, A. Kucernak, *Electrochem. Commun.* **2017**, *83*, 67.

[18] a) M. Khalil, M. A. Marcus, A. L. Smeigh, J. K. McCusker, H. H. W. Chong, R. W. Schoenlein, *J. Phys. Chem. A* **2006**, *110*, 38; b) T. E. Westre, P. Kennepohl, J. G. DeWitt, B. Hedman, K. O. Hodgson, E. I. Solomon, *J. Am. Chem. Soc.* **1997**, *119*, 6297; c) G. Rossi, F. d'Acapito, L. Amidani, F. Boscherini, M. Pedio, *Phys. Chem. Chem. Phys.* **2016**, *18*, 23686.

[19] J. J. Rehr, J. J. Kas, M. P. Prange, A. P. Sorini, Y. Takimoto, F. Vila, *C. R. Phys.* **2009**, *10*, 548.

[20] G. Wu, K. L. More, C. M. Johnston, P. Zelenay, *Science* **2011**, *332*, 443.

[21] C. Zheng, K. Mathew, C. Chen, Y. Chen, H. Tang, A. Dozier, J. J. Kas, F. D. Vila, J. J. Rehr, L. F. J. Piper, K. A. Persson, S. P. Ong, *npj Comput. Mater.* **2018**, *4*, 12.

[22] M. Ferrandon, A. J. Kropf, D. J. Myers, K. Artyushkova, U. Kramm, P. Bogdanoff, G. Wu, C. M. Johnston, P. Zelenay, *J. Phys. Chem. C* **2012**, *116*, 16001.

[23] A. Zitolo, V. Goellner, V. Armel, M.-T. Sougrati, T. Mineva, L. Stievano, E. Fonda, F. Jaouen, *Nat. Mater.* **2015**, *14*, 937.

[24] H. Fei, J. Dong, Y. Feng, C. S. Allen, C. Wan, B. Volosskiy, M. Li, Z. Zhao, Y. Wang, H. Sun, P. An, W. Chen, Z. Guo, C. Lee, D. Chen, I. Shakir, M. Liu, T. Hu, Y. Li, A. I. Kirkland, X. Duan, Y. Huang, *Nat. Catal.* **2018**, *1*, 63.

[25] J.-Y. Gu, Z.-F. Cai, D. Wang, L.-J. Wan, *ACS Nano* **2016**, *10*, 8746.

[26] S. H. Kim, O. Toshiaki, G. H. Gang, *Bull. Korean Chem. Soc.* **2000**, *21*, 588.

[27] M. Bron, J. Radnik, M. Fieber-Erdmann, P. Bogdanoff, S. Fiechter, *J. Electroanal. Chem.* **2002**, *535*, 113.

[28] H. Zhang, S. Hwang, M. Wang, Z. Feng, S. Karakalos, L. Luo, Z. Qiao, X. Xie, C. Wang, D. Su, Y. Shao, G. Wu, *J. Am. Chem. Soc.* **2017**, *139*, 14143.